On the numerical modeling of track-etched membranes used as collimators of the X-ray radiation

© A.V. Mitrofanov, R.M. Feshchenko

Lebedev Physical Institute, Russian Academy of Sciences,
119991 Moscow, Russia
e-mail: rusl@sci.lebedev.ru

In this work, we present the results of numerical modeling of distribution of the field amplitude inside micronsized through cylindrical pores in polymer track membranes in the soft X-ray wavelength range $13.5-30.4$ nm. The calculations were performed by numerically solving the $3D$-parabolic equation with a finite-difference method using an exact transparent boundary condition. The dependences of the X-ray transmittivity through a pore on the incidence angle as well as on the pore diameter were computed. For the membranes with some thicknesses and pore diameters calculated angular dependences of the transmittance are compared with the measurements known from the literature. It is demonstrated that the calculations agree with the measurements if a transition layer on the inner surface of the pores, which accounts for the finite surface roughness, is introduced.

Keywords: X-ray optics, solar astronomy, filters, parabolic equation.

Introduction

Polymer track membranes with through pores of a micrometer or submicrometer diameter [1,2] and microstructured heterogeneous thin-film objects based on them are used widely as optical elements in the soft X-ray and vacuum ultraviolet ranges (at wavelengths ranging from 1 to 100 nm) [3–7]. Specifically, they may serve as diffraction filters of solar X-ray radiometers [3], filters in imaging soft X-ray optics, high-strength supports for thin-film X-ray filters, compact heatsinks for heat dumping in vacuum, collimators, etc. [4–7]. The key function of such filters is to protect a detector from intense direct and lateral background illumination (in most cases, by long-wavelength radiation of the studied object, such as the Sun, or by reflected ultraviolet, visible, and infrared radiation). However, it is known that the optical characteristics of track membranes depend strongly on the angle of radiation incidence onto a sample. This necessitates the use of complex methods for calculation of these characteristics.

The aim of the present study is to model numerically the transmission of soft X-ray radiation through cylindrical micropores in polymer films and compare the obtained results with measured angular transmission characteristics of track membrane samples in the soft X-ray range at certain operating wavelengths of an X-ray solar telescope [7]. it should be noted that the collimating properties of polyethylene terephthalate (PET) track membranes in the $100-200$ nm ultraviolet range have been examined earlier in [8,9].

The soft X-ray range considered in the present study contains the operating spectral lines of solar telescope instruments designed for coronal plasma imaging in Fe IX−Fe XI lines and the He II 30.4 nm line [7].

1. Numerical modeling of a cylindrical waveguide

The transmission of soft X-ray radiation with wavelengths of 13.5, 17.06, and 30.4 nm within a through cylindrical pore in a PET membrane was examined using a three-dimensional parabolic wave equation of the following form:

$$2ik\,\frac{\partial u}{\partial z} = -\frac{\partial^2 u}{\partial x^2} - \frac{\partial^2 u}{\partial y^2} - k^2\big(\varepsilon(x,y)-1\big)u, \qquad (1)$$

where u is the field amplitude, x, y, z are Cartesian coordinates, $\varepsilon(x,y) = n^2 = 1-2\delta + 2i\beta$ is the complex permittivity of PET, $k = 2\pi/\lambda$ is the wave number, λ is the wave length, and n is the refraction index. The electrical field of a wave may then be written as $E = e^{-i\omega t + ikz}u$. Optical constants δ and β for PET were taken from [10].

The calculation methods used in this study are the result of further development of techniques from [11], where a $2D$ parabolic equation was applied in the simulation of radiation transmission through cylindrical pores under normal incidence of X-ray radiation onto a film. The transition to $3D$ parabolic equation (1) provides an opportunity to characterize both the transmission of radiation incident at a nonzero angle to the surface normal through cylindrical pores and the transmission of radiation through cylindrically asymmetric pores. Just as in [11], parabolic equation (1) was solved using the unconditionally stable Crank−Nicolson finite-difference method; however, this time it was done in a rectangular computational domain. The so-called exact transparent boundary condition for a rectangular computational domain was applied [9,12]. The method of splitting of the two-dimensional Laplace operator at the right-hand side of Eq. (1) with subsequent application of $1D$ finite-difference schemes was used to speed up the
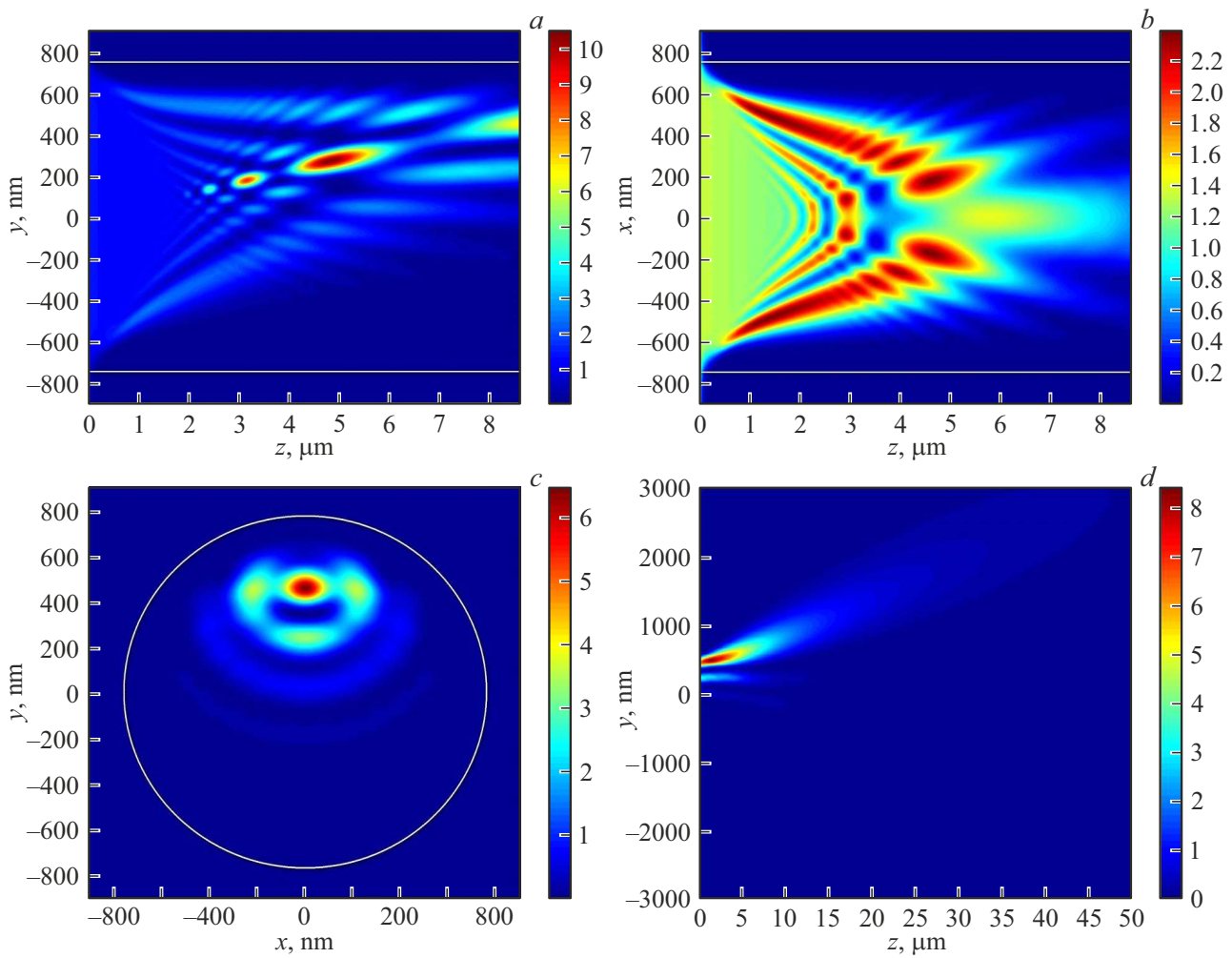
Figure 1. Results of simulation of the transmission of X-ray radiation with a wavelength of 30.4 nm through a pore with its walls smoothed by function (2) ($\mu = 1$) at an incidence angle of 0.06 rad. Distributions of absolute field amplitude squared $|u|^2$ in three orthogonal planes (*a–c*) and in free space in the vertical plane (*d*) are shown in a linear scale. The color scale is to the right of the figures. White horizontal lines are the boundaries of a pore 1500 nm in diameter.

calculations. All calculations were carried out with the use of codes developed specifically for this purpose in Matlab.

A rectangular computational domain with a size 20% greater than the pore diameter was chosen to model the transmission of radiation through a pore. For example, this size was 1800×1800 nm for a pore diameter of 1500 nm. The step in lateral coordinates (x, y), which are measured from the pore axis, and longitudinal coordinate z was 4 and 10 nm, respectively, in all cases. A sample with a pore was irradiated by a plane wave incident at angle θ in plane (y, z). Coefficient of transmission T through a pore was calculated as the ratio of the total radiation flux passing through the entire square computational domain at the last modeling step to the radiation flux incident onto the inlet of a pore.

In order to obtain a better fit to experimental data, the boundaries between pore walls and vacuum were assumed

not to be sharp with blurring characterized by function

$$\varepsilon(r) = \frac{\varepsilon_1}{2} \mu \left(2 - \mathrm{erfc}\left(\left(\frac{d^2}{4} - r^2 \right) \frac{1}{Dd} \right) \right)$$
$$+ \frac{\varepsilon_1}{2} (1 - \mu) \left(1 + \theta\left(\frac{d^2}{4} - r^2 \right) \right), \qquad (2)$$

which is a sum of a step (with weight fraction $0 < \mu < 1$) and a blurred layer with transition thickness d, where the error function is

$$\mathrm{erfc}(x) = \frac{2}{\sqrt{\pi}} \int\limits_{x}^{\infty} e^{-t^2} dt,$$

and ε_1 is the permittivity of solid PET. This representation of the behavior of permittivity in the vicinity of a pore wall provides, among other things, an opportunity to characterize

phenomenologically the influence of the wall surface roughness on the coefficient of radiation transmission through a pore. Specific d values were chosen simply by cycling through various values of the blurring thickness. It should be noted that the influence of transition layers on the waveguide characteristics has been examined in [13].

Further propagation of radiation in free space beyond a pore was modeled using a finite-difference scheme for 3D parabolic equation (1), where $\varepsilon = 1$. The size of the computational domain in these calculations was four times greater than the pore diameter. The lateral and longitudinal step was 12 and 96 nm, respectively.

Squared values of the field amplitude in three orthogonal planes calculated for radiation with a wavelength of 30.4 nm propagating within a pore with diameter $D = 1500$ nm and length $L = 8600$ nm are shown in Figs. 1, a–c. The incidence angle is $\theta = 0.06$ rad, the transition layer thickness is $d = 42$ nm, and parameter $\mu = 1$ in (2). Partial channeling and focusing of radiation within a pore, reflection off walls, and interference of incident and reflected waves are especially pronounced in Fig. 1, a. Figure 1, b reveals a complex structure of the field in the horizontal plane. The distribution of radiation at the pore outlet in Fig. 1, c has a complex asymmetric structure. Figure 1, d shows the field amplitude squared in free space beyond the pore that is depicted in Figs. 1, a–c.

2. Examination of transmission through a pore as a function of various parameters

Coefficients of transmission T through a pore calculated for wavelengths of 17.06 and 30.4 nm are presented in Fig. 2 as functions of incidence angle θ. Measured coefficients for the same wavelengths (and, for comparison, a wavelength of 58 nm) and the results of calculation by formula

$$T = \frac{1}{\pi}\left[2\sin^{-1}\sqrt{1 - \left(\frac{L}{D}\tan\theta\right)^2} \right.$$
$$\left. - \frac{2L}{D}|\tan\theta|\sqrt{1 - \left(\frac{L}{D}\tan\theta\right)^2}\right], \qquad (3)$$

which characterizes the transmission of radiation through a pore with nonreflective walls in the geometric approximation, are also shown in Fig. 2. The experimental plots were normalized to unity at $\theta = 0$.

It can be seen that a pore with ideal walls should, according to calculated data, feature a considerable transmittance at large incidence angles (up to the critical ones for the corresponding wavelengths). The measured coefficients of transmission of track membranes are characterized well by simple geometric formula (3). It is also evident that a good agreement between the results of numerical calculations and measurements is achieved at a wavelength of 17.06 nm if permittivity blurring within a
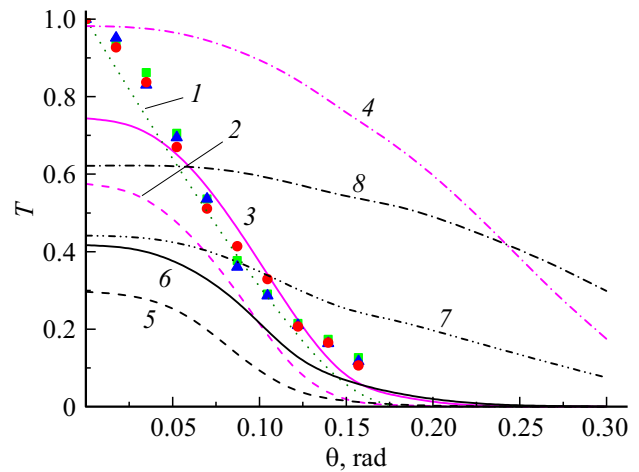
Figure 2. Calculated and measured [6] coefficients of transmission through a pore in a PET film as functions of the angle of radiation incidence for various wavelengths. The measurement data for wavelengths $\lambda = 17.06$, 58.5, and 30.4 nm are represented by squares, triangles, and circles, respectively. Curves correspond to the results of calculations performed using various models with different parameters: 1 — formula (3); 2 — $\lambda = 17.06$ nm, $d = 61$ nm; 3 — $\lambda = 17.06$ nm, $d = 42$ nm; 4 — $\lambda = 17.06$ nm, $d = 0$ nm; 5 — $\lambda = 30.4$ nm, $d = 61$ nm; 6 — $\lambda = 30.4$ nm, $d = 42$ nm; 7 — $\lambda = 30.4$ nm, $d = 42$ ($\mu = 1/2$) nm; 8 — $\lambda = 30.4$ nm, $d = 0$ nm (see Eq. (2)).

layer with thickness $d = 42$ nm ($\mu = 1$ in formula (2)) at the inner pore surface is introduced into the model. At a wavelength of 30.4 nm, the same blurred layer thickness yields a somewhat underestimated value of the coefficient of transmission, and the best fit to measurements is provided by the model with $d = 30$ nm. As for the model with a halved step layer ($\mu = 1/2$ in formula (2)), it does not improve the quality of the fit. This behavior of calculated reflection coefficients may be attributed to limitations of chosen models of the transition layer or to the use of inaccurate values of permittivity at a wavelength of 30.4 nm.

Figure 3 presents the dependence of transmittance of a pore on its radius ($D/2$) at three different wavelengths for the transition layer model used in Fig. 2 ($d = 42$ nm and $\mu = 1$). It can be seen that the transmittance is virtually zero at $D/2 < 100$ nm, grows rapidly with increasing radius following a law typical for small pores, and then gradually approaches saturation.

3. Modeling of reflection from a plane boundary

In order to clarify the influence of a transition layer on the transmission of radiation through a pore, the coefficient of reflection of radiation from a plane boundary with a transition layer (specified by formula (2)) and without it was calculated. An one-dimensional wave equation

$$E_{zz}'' + k^2\big(\varepsilon(z) - \cos^2\theta\big)E = 0 \qquad (4)$$

for the electrical field of a wave was solved numerically for this purpose by reducing (4) to a Riccati equation with subsequent numerical finite-difference integration.

The results of calculations for a wavelength of 30.4 nm are shown in Fig. 4. It can be seen that the coefficient of reflection decreases appreciably and fairly monotonically following the introduction of transition layers of a varying thickness with different weight coefficients of a step transition (parameter μ in (2)). This reduction is the cause of a sharp drop in transmittance of pores at large angles of radiation incidence onto a film.

Figure 5 concludes the study with a comparison of the coefficients of reflection from plane surface calculated using Eq. (4) and a simple model of a rough surface based on the
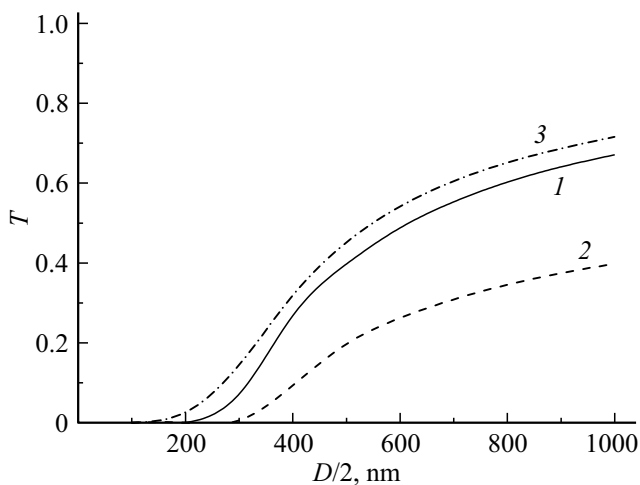
Figure 3. Calculated coefficient of transmission through a pore in a PET film as function of the pore radius for wavelengths λ, nm: 1 — 17.06; 2 — 30.4; 3 — 13.31; $d = 42$ nm, $\mu = 1$ (see Eq. (2)).
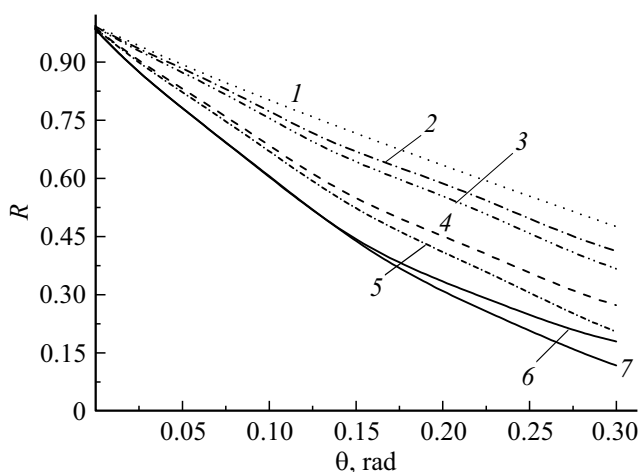
Figure 4. Coefficients of reflection from plane continuous PET films at a wavelength of 30.4 nm as functions of the grazing angle for different model parameters of the transient layer characterized by formula (2) and for Fresnel reflection from a sharp boundary: 1 — Fresnel coefficient; 2 — $d = 10$ nm, $\mu = 1$; 3 — $d = 10$ nm, $\mu = 0.5$; 4 — $d = 21$ nm, $\mu = 1$; 5 — $d = 21$ nm, $\mu = 0.5$; 6 — $d = 30$ nm, $\mu = 1$; 7 — $d = 30$ nm, $\mu = 0.5$.
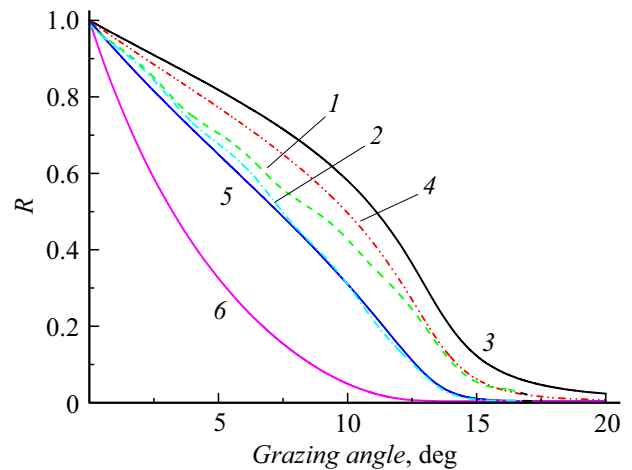
Figure 5. Coefficients of reflection from plane continuous PET films at a wavelength of 13.5 nm as functions of the grazing angle for different model parameters of the transient layer characterized by formula (2) (1 — $\mu = 0.5$, $d = 42$ nm; 2 — $\mu = 1$, $d = 42$ nm) and for Debye reflection model (5) (3 — $\sigma = 0$ nm; 4 — $\sigma = 5$ nm; 5 — $\sigma = 10$ nm; 6 — $\sigma = 20$ nm).

Debye−Waller factor

$$dw = \exp\left(-\left(\frac{4\pi \sin\theta}{\lambda}\right)^2 \sigma^2\right) \qquad (5)$$

with root-mean-square roughness σ. It is evident the model discussed in the present study with a transition layer thickness $d = 42$ nm corresponds to the model of a surface with $\sigma = 10$ nm.

Conclusion

Numerical modeling of the transmission of soft X-ray radiation through cylindrical pores in a PET film was performed with the use of a 3D parabolic equation, an exact transparent boundary condition, and the finite-difference method. Dependences of the transmittance on the angle of radiation incidence and the pore diameter were calculated with a finite roughness of the inner surface of a pore taken into account. The results of transmittance calculations were found to agree with measurement data for a wavelength of 17.06 nm at a specific selected value of the transition layer thickness. It was demonstrated through calculations of the coefficient of reflection from a plane surface that this is attributable to a significant reduction in the coefficient of reflection of soft X-ray radiation from a pore wall at the used values of the transition layer thickness.

The obtained results suggest that the method of solving a 3D parabolic equation with the use of finite-difference schemes may find practical applications in calculations of characteristics of thin-film X-ray collimators based on track membranes with through pores with different features of the pore wall microrelief (including polymer samples fabricated from polycarbonate and polyimide track membranes, which are known to have pores with smooth walls).

Acknowledgments

Conflict of interest

The authors declare that they have no conflict of interest.

References

[1] G.N. Flerov, V.S. Barashenkov. Sov. Phys. Usp. **17** (5), 783−793 (1974).
DOI: 10.1070/PU1975v017n05ABEH004371

[2] P.Yu. Apel, S.N. Dmitriev. Track In: *Membranes and membrane technology,* ed. by A.B. Yaroslavtsev (Science World, M., 2013), p. 117−160. (in Russian)

[3] M. Dominique, A.V. Mitrofanov, J.-F. Hochedez, P.Yu. Apel, U. Schühle, F.A. Pudonin, O.L. Orelovich, S.Yu. Zuev, D. Bolsée, C. Hermans, A. BenMoussa. Appl. Opt., **48** (5), 834 (2009). DOI: 10.1364/AO.48.000834.

[4] A.V. Mitrofanov. Quant. Electron., **48** (2), 105−110 (2018). DOI: 10.1070/QEL16540

[5] A.V. Mitrofanov, P.Yu. Apel. Nucl. Instrum. Meth. B, **245**, 332 (2006). DOI: 10.1070/QEL16540

[6] A.V. Mitrofanov, P.Y. Apel. Bull. Russ. Acad. Sci. Phys., **73** (1), 57 (2009). DOI: 10.3103/S106287380901016X

[7] *Solar-Terrestrial Physics: Results of the Experiments of Koronas-F Satellite,* ed. by V.D. Kuznetsov (Physmatlit, M., 2009), p. 73 (in Russian)

[8] A.V. Mitrofanov. Insrum. Experim. Tech., **27** (4), 966 (1984).

[9] A.V. Mitrofanov, R.M. Feshchenko. Bull. Lebedev Phys. Inst., **49** (6), 169−173 (2022). DOI: 10.3103/S1068335622060057

[10] X-Ray Interactions with Matter [Electronic source] Electron. data Center for X-Ray Optics. Lawrence Berkeley National Laboratory, 2010 Available at: www.cxro.lbl.gov/optical_constants, open access.

[11] A.V. Mitrofanov, A.V. Popov, D.V. Prokopovich. Radioelectronics. Nanosystems. Information Technologies, **12** (2), 173 (2020). DOI: 10.17725/rensit.2020.12.173 (in Russian)

[12] R.M. Feshchenko, A.V. Popov. Phys. Rev. E, **104** (2), 025306 (2021). DOI: 10.1103/PhysRevE.104.025306

[13] V.A. Bushuev, O.D. Roshchupkina. Bull. Russ. Acad. Sci. Phys., **71** (1), 59 (2007). DOI: 10.3103/S1062873807010157

Translated by D.Safin